Measurement of the ion drag force in a collisionless plasma with strong ion-grain coupling

V. Nosenko
Max-Planck-Institut für extraterrestrische Physik, D-85741 Garching, Germany

R. Fisher and R. Merlino
Department of Physics and Astronomy, The University of Iowa, Iowa City, Iowa 52242, USA

S. Khrapak and G. Morfill
Max-Planck-Institut für extraterrestrische Physik, D-85741 Garching, Germany

K. Avinash
Department of Physics and Astrophysics, University of Delhi, Delhi-7, India

(Received 22 June 2007; accepted 21 August 2007; published online 8 October 2007)

The ion drag force acting on dust grains was measured experimentally in a low-pressure Ar plasma in the regime of strong ion-grain coupling. Argon ions were drifting in the axial ambipolar electric field naturally present in a hot-filament dc discharge plasma. Following the method of Hirt *et al.* [Phys. Plasmas **11**, 5690 (2004)], hollow glass microspheres were dropped into the plasma and allowed to fall due to gravity. The ion drag force was derived from the particle trajectory deflection from the vertical direction. The result is in reasonable agreement with a theoretical model that takes strong ion-grain coupling into account. © *2007 American Institute of Physics*.
[DOI: 10.1063/1.2783221]

I. INTRODUCTION

The ion drag force arises whenever a flow of ions encounters an obstacle. When the momentum of a drifting ion changes due to its interaction with an object, the ion exerts a force on that object. The ion drag force is important in plasma applications where microparticle transport is involved[1–3] and in complex plasmas, where it is responsible for the formation of voids.[4–10] It has also been discussed in novel medical diagnostics methods.[11]

Despite the high importance of the ion drag force in complex plasmas, a complete self-consistent model for this force, describing all cases of interest, has not yet been developed. Rather, there exist several approaches, which can be utilized under certain well defined conditions. Therefore, when one compares an experimentally measured ion drag force to a theoretical calculation, it is important to use a suitable theoretical model that is valid in a given experimental situation.

The ion drag force acting on dust particles immersed in a plasma was measured in a number of experiments.[12–17] However, only one experiment[14,15] was carried out in the regime where ions were completely collisionless with respect to collection and scattering by the grains, whereas the majority of reliable theoretical results were obtained for collisionless ions. In Refs. 14 and 15, a fixed (low) pressure of 7×10^{-2} Pa (0.53 mTorr) was used;[18] the ion drift velocity was suprathermal.

In the present paper, we report a measurement of the ion drag force acting on dust grains in a collisionless plasma with strong ion-grain coupling. We varied experimental parameters, including the neutral gas pressure, so that the ion drift velocity ranged from subthermal to slightly suprathermal. A theoretical model based on the approach of Ref. 19 is developed that is suitable for our experimental conditions. A reasonable agreement is found between our experiment and theory.

II. EXPERIMENTAL METHOD

To measure the ion drag force, we used the method of Ref. 15. Dust particles were dropped into a dc discharge plasma. As they fell due to gravity, their trajectories were deflected from the vertical direction due to the ion drag force; all other forces were negligibly small. In this situation, the ion drag force is easily calculated from the particle mass and the angle of deflection.

We used a hot-filament direct current (dc) discharge with multidipole magnetic confinement[20] (see Fig. 1). The vacuum chamber is a stainless steel cylinder with a diameter of 60 cm and length of 90 cm. The cathode is a hot tungsten wire; the anode is the inside surface of the (grounded) vacuum chamber. The actual area of the chamber surface that is in contact with plasma is greatly reduced due to the multidipole magnetic confinement. As a result, the plasma loss to the chamber walls is low and a relatively high plasma density can be achieved at low gas pressures. The plasma chamber was equipped with a planar Langmuir probe that could be moved along its axis. This allowed us to measure the axial profiles of the plasma parameters.

The particles were introduced into plasma from a small container mounted near the chamber top. As they fell, they were illuminated by a vertical sheet of laser light and imaged with an analog video camera viewing normal to the laser sheet. We used a red laser diode emitting at 681 nm; the camera was equipped with a corresponding bandpass interference filter, so that only the laser light scattered from par-

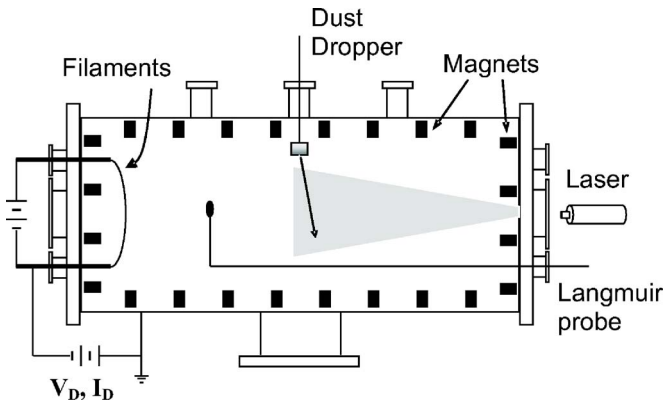

FIG. 1. Experimental setup. Glass particles are deflected by the ion drag force as they fall in a plasma. The plasma is produced in a hot-filament dc discharge with multidipole magnetic confinement.

ticles was admitted into camera. The camera operated at 29.97 frames per second.

The experimental parameters were as follows. We used Ar at low pressure of 0.2–0.8 mTorr. The discharge voltage was fixed at 60 V, while the discharge current could be varied in the range of 0.2–2.2 A by changing the hot filament current. We used hollow glass microspheres having an average mass density of 0.35 g/cm^3. Microspheres of two different diameters were used: 40 ± 4 μm and 59 ± 15 μm (we call them the smaller and bigger particles, respectively). The neutral-gas damping rate was in the range of $\gamma=0.02-0.12$ s^{-1}, as modeled[21] by the Epstein expression.

Our primary experimental measurement was the angle of deflection of the particle trajectories from the vertical direction measured near the chamber axis. We analyzed experimental movies frame by frame. The particle trajectories appeared as long straight lines. The angle of deflection α was measured for 80–200 particle trajectories, for every set of experimental conditions (40–50 trajectories for the lowest discharge pressure and current). The angle α had a distribution that we modeled by a Gaussian with a mean value of α_0 and standard deviation of $\sigma_\alpha=(0.3-0.6)\alpha_0$ (up to α_0 at the lowest discharge current). The large scatter in the values of the trajectory angle is due to the big spread in the particle size and their initial velocities as they leave the particle container. The error in calculating α_0 did not exceed 10%.

We assume that the particle motion is determined by gravity and the ion drag force. We verified that the thermophoretic force did not play a role in our experiment by switching the discharge voltage off, while leaving the filaments on. In this test, there was no plasma, but the thermophoretic force (if any) should have been the same. The particles were not deflected in this test, ruling the thermophoretic force out. The neutral drag force can be neglected, because the measured particle speed was much smaller than the terminal speed $v_{\text{term}}=g/\gamma$. (In addition, there was no deflection of particles in a test where we admitted argon into chamber, but did not make a discharge.) The assumption that the electric force is much smaller than the ion drag force is verified toward the end of the paper.

III. MEASUREMENT OF THE ION DRAG FORCE

We measured the ion drag force for various combinations of experimental parameters. In one series of measurements, we fixed the pressure of argon at 0.6 mTorr and varied the discharge current in the range of 0.2–2.2 A by adjusting the hot filament current. Both bigger and smaller particles were used. In another series of measurements, we kept the discharge current constant at 1.4 A while varying the argon pressure in the range of 0.2–0.8 mTorr. Bigger particles were used in this case.

Using the movable Langmuir probe, we measured the axial profiles of the plasma potential, plasma density, and electron temperature. For the experiment with constant argon pressure (0.6 mTorr), the results are shown in Fig. 2. We adopt the usual assumption for such plasmas that the argon ions and neutral atoms are approximately at room temperature: $T_i\approx T_n\approx 0.03$ eV. The plasma potential had a weak axial gradient, as in Fig. 2(a). The corresponding electric field was directed horizontally away from the hot filaments and had a magnitude of the order of a few volts per meter. Ar^+ ions drifted in this field and exerted a drag force on the falling particles.

We calculate the ion drag force as $F_i=mg\tan\alpha_0$, where m is the particle mass and α_0 is the angle of the particle trajectory deflection from the vertical direction. The results are shown in Fig. 3 (solid circles) and in Tables I and II, where we also summarize our experimental measurements of the plasma parameters, as well as theoretical calculations from Sec. IV.

To compare our experimental results to theoretical calculations, we should use a theoretical model that is valid for collisionless plasmas with strong ion-grain coupling, where the ion drift velocity can be either subthermal or suprathermal (see Tables I and II). The most suitable model is that of Ref. 19; however, it allows only subthermal ions and does not specify the value of the effective plasma screening length. Therefore, in the next section we extend the model of Ref. 19 to the regime of suprathermal ions and evaluate the effective screening length to be used under the conditions studied.

IV. THEORY

In this section we first briefly review the current level of the theoretical research (for more details, see, e.g., Refs. 8, 9, 22, and 23), specify main assumptions and simplifications, and then derive an analytical approximation relevant to the conditions of the present experiment.

The traditional way to derive the ion drag force is the "binary collision (BC) approach," which is based on the solution of the mechanical problem of the ion motion in the field of the particle. Analysis of ion trajectories yields the velocity-dependent momentum transfer cross section $\sigma(v)$. The force can be then obtained by integrating $\sigma(v)$ with an appropriate ion velocity distribution function.[24] Typical assumption used in BC approach is the isotropic attractive Debye-Hückel (Yukawa) interaction potential between the ions and the grain. An important quantity characterizing momentum transfer in the Yukawa potential is the so-called

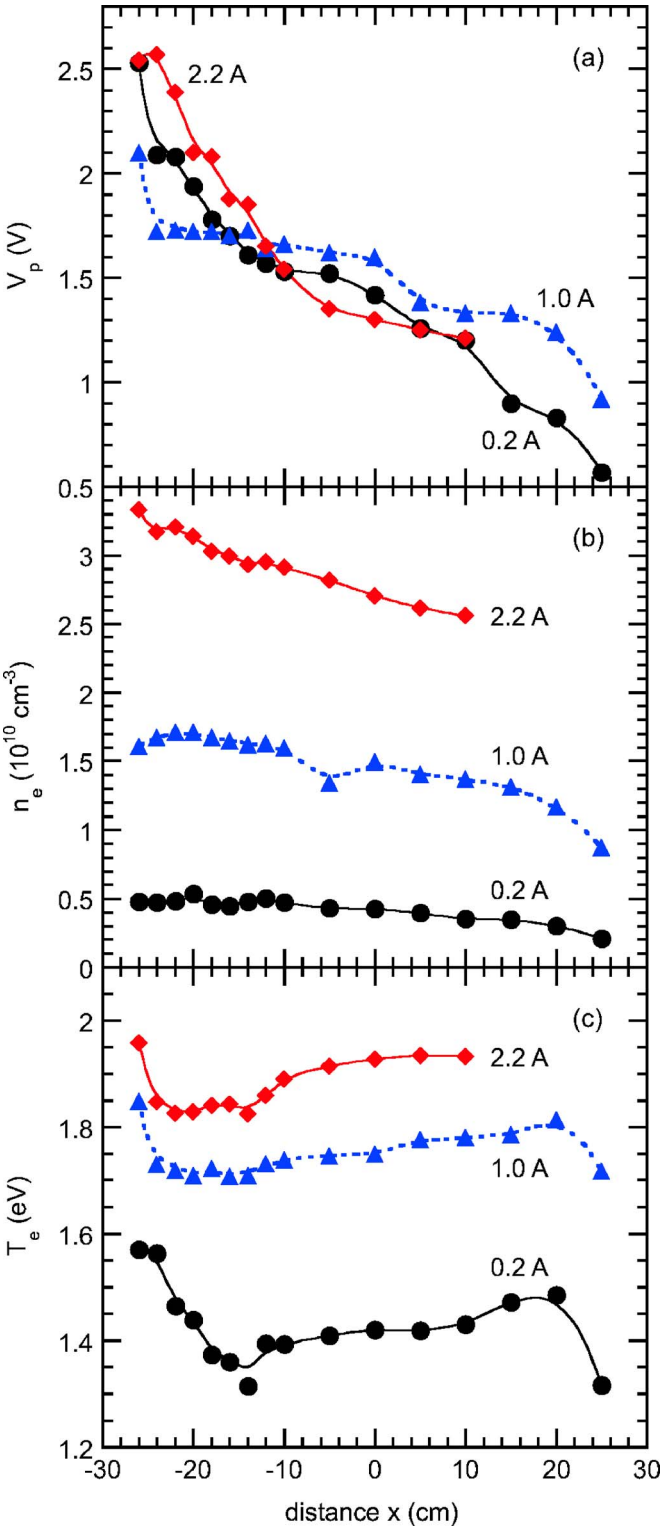

FIG. 2. (Color online) Axial profiles of the plasma potential (a), plasma density (b), and electron temperature (c) for a discharge in argon at 0.6 mTorr; the discharge current was varied in the range of 0.2–2.2 A. The distance $x=0$ corresponds to the location of falling particles.

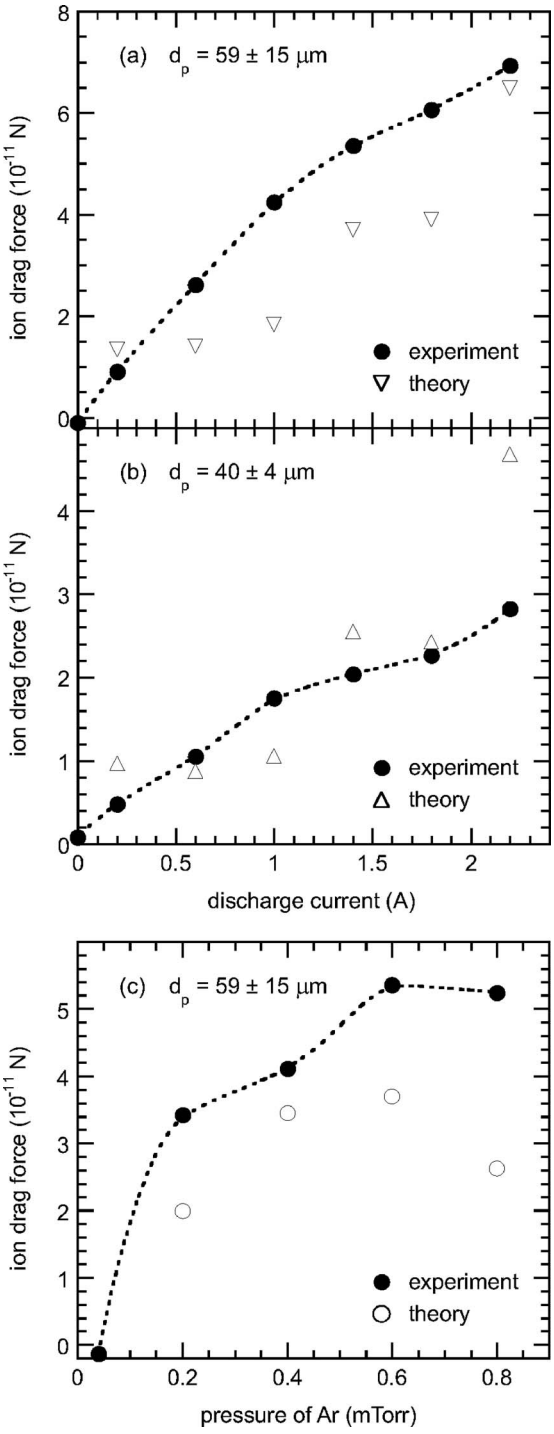

FIG. 3. Ion drag force as a function of discharge current [(a), (b)] and discharge pressure (c). In (a) and (b), the pressure of argon was fixed at 0.6 mTorr; in (c), the discharge current was kept constant at 1.4 A. Bigger particles (diameter 59±15 μm) were used in (a) and (c); smaller particles (diameter 40±4 μm) were used in (b). Experimental measurements are shown by solid circles and theoretical calculations using formula (4) are shown by open symbols. Parameters used in calculations are summarized in Tables I and II.

scattering parameter, $\beta=(e|\phi_s|/m_iv^2)(a/\lambda)$, where ϕ_s is the grain surface potential, a is the grain radius, λ is the *effective* screening length, m_i is the ion mass, and v is the ion velocity. This parameter is a measure of the strength of "ion-grain coupling" and determines how the momentum transfer occurs. For weak coupling ($\beta \ll 1$), the length scale of nonlinear interaction and scattering at large angles ($\sim e|\phi_s|a/m_iv^2$) is much shorter than the screening length. In this regime the conventional Coulomb scattering theory (small-angle scattering approximation) is applicable. An ex-

TABLE I. Experimentally measured and theoretically calculated parameters evaluated at the location of falling particles for a discharge in argon at 0.6 mTorr. The numbers before and after the slash correspond respectively to the bigger particles (diameter 59±15 μm) and smaller particles (diameter 40±4 μm).

Discharge current (A)	0.2	0.6	1.0	1.4	1.8	2.2
			Experimentally measured parameters			
Plasma density n (10^{10} cm^{-3})	0.43	0.96	1.49	1.94	2.32	2.70
Electron temperature T_e (eV)	1.4	1.6	1.7	1.8	2.0	1.9
Electric field E (V/m)	2.2	0.9	0.7	2.6	1.7	4.4
Deflection angle α_0 (°)	1.41/2.30	4.07/4.98	6.57/8.27	8.27/9.60	9.34/10.63	10.65/13.21
Ion drag force F_i (10^{-11} N)	0.91/0.48	2.62/1.05	4.24/1.75	5.36/2.04	6.07/2.26	6.93/2.83
			Calculated parameters			
Ion drift velocity $u_0=u/v_{T_i}$	1.4	0.7	0.6	1.6	1.2	2.4
Dimensionless grain surface potential $z=e\lvert\phi_s\rvert/T_e$	2.9	2.7	2.7	2.9	2.7	3.0
Screening length λ (μm)	61/57	51/42	51/40	39/34	41/33	37/34
Scattering parameter β_{av}	21/16	56/46	67/57	36/28	55/45	24/17
Ion drag force F_i (10^{-11} N)	1.34/0.97	1.40/0.87	1.83/1.06	3.70/2.55	3.90/2.43	6.49/4.68

tension of the Coulomb scattering theory to the regime of moderate coupling ($\beta\sim 1$) has been proposed in Ref. 24, where the fact that the interaction range can be comparable or even exceeds the screening length has been accounted for. This requires a proper choice of the upper cutoff impact parameter and basically leads to a modification of the Coulomb logarithm. In the case of strong coupling ($\beta\gg 1$) the interaction range considerably exceeds λ and most of the contribution to the momentum transfer is from scattering with large angles.[19,22] Thus, BC approach is applicable for any degree of the ion-grain coupling, but since it operates with ballistic ion trajectories the effect of ion-neutral collisions, which is often important in complex plasmas cannot be consistently accounted for.

An alternative way to calculate the ion drag force is based on the so-called "linear dielectric response formalism." Instead of calculating single ion trajectories and then the momentum transfer cross section, one can solve the Poisson equation coupled to the kinetic (or hydrodynamic) equations for the ions and electrons and obtain the self-consistent anisotropic component of the electric field induced by the ion flow at the position of the grain, which produces the (drag)

TABLE II. Experimentally measured and theoretically calculated parameters evaluated at the location of falling particles for a discharge current of 1.4 A and bigger particles (diameter 59±15 μm).

Pressure of Ar (mTorr)	0.2	0.4	0.6	0.8
		Experimentally measured parameters		
Plasma density n (10^{10} cm^{-3})	0.74	1.43	1.94	1.82
Electron temperature T_e (eV)	2.4	2.0	1.8	1.7
Electric field E (V/m)	0.35	1.7	2.6	1.8
Deflection angle α_0 (°)	5.30	6.36	8.27	8.09
Ion drag force F_i (10^{-11} N)	3.42	4.11	5.36	5.24
		Calculated parameters		
Ion drift velocity $u_0=u/v_{T_i}$	0.8	1.6	1.6	1.0
Dimensionless grain surface potential $z=e\lvert\phi_s\rvert/T_e$	2.6	2.8	2.9	2.7
Screening length λ (μm)	64	44	39	42
Scattering parameter β_{av}	58	35	36	55
Ion drag force F_i (10^{-11} N)	1.99	3.45	3.70	2.63

force on the grain.[9,23,25–27] This approach consistently accounts for ion-neutral collisions and potential anisotropy caused by the ion flow, uses the ion velocity distribution function calculated self-consistently, but is applicable only for the weak ion-grain coupling, $\beta \ll 1$.

In the experiment described in this paper ions are collisionless with respect to collection and scattering by the grains. The characteristic ion mean free path at the highest pressure of 0.8 mTorr is $\ell_i \sim 2$ cm. The plasma density ranges from $\sim 2\times 10^9$ to $\sim 2\times 10^{10}$ cm^{-3} yielding the ion Debye radii between 10 and 30 μm, assuming that the ions are at room temperature. Three orders of magnitude difference between ℓ_i and λ_{Di} allow us to completely neglect any collisional effect either on grain charging or on the ion drag force. For this reason, in this paper we stick to the BC approach to describe ion-grain collisions.

On length scales larger than the ion mean free path the ion motion is mobility limited. The relation between the ion flow velocity u and the electric field E is given by the ion mobility μ (which is a function of the electric field): $u=\mu E$. For argon ion mobility in argon gas, we adopt the approximation of Frost,[28] $\mu(E)=\mu_0 p^{-1}[1+\alpha(E/p)]^{-1/2}$, where $\mu_0=1460$ cm^2/V, p is pressure in Torr, and $\alpha=0.0264$ cm/V. For the electric fields measured in the experiment (between 0.4 and 4.4 V/m) the ratio of the ion drift velocity to the ion thermal velocity ($u_0=u/v_{T_i}$) is between 0.6 and 2.4; i.e., the ion drift is nearly thermal. Nevertheless, in calculating the grain surface potential and ion drag force the ion flow velocity is allowed to be arbitrary. The only simplification involved is the assumption of shifted Maxwellian distribution function. Possible deviations are not expected to be very important as long as u_0 is not large.[26]

The grain surface potential can be estimated as follows. It has been recently demonstrated that the flow induced asymmetry in the ion-grain interaction is a neither large nor dominant effect with respect to charging process.[29,30] The ion and electron fluxes collected by the grain can be therefore evaluated using the conventional orbital motion limited (OML) approach. For stationary electron background and shifted-Maxwellian ions, the corresponding expressions are[31,32]

$$J_e = \sqrt{8\pi} a^2 n_e v_{T_e} \exp(-z),$$
$$J_i = \sqrt{2\pi} a^2 n_i v_{T_i} u_0^{-1} \left[\sqrt{\frac{\pi}{2}} (1 + u_0^2 + 2z\tau) \operatorname{erf}\left(\frac{u_0}{\sqrt{2}}\right) + u_0 \exp\left(-\frac{u_0^2}{2}\right)\right]. \quad (1)$$

Here, $n_{i(e)}$ and $T_{i(e)}$ are the ion (electron) density and temperature, respectively, $v_{T_{i(e)}}=\sqrt{T_{i(e)}/m_{i(e)}}$ is the ion (electron) thermal velocity, $z=e|\phi_s|/T_e$ is the dimensionless surface potential, and $\tau=T_e/T_i$ is the electron-to-ion temperature ratio. The flux balance condition $J_e=J_i$ yields the value of the dimensionless grain surface potential as a function of the normalized ion flow velocity u_0 (see Tables I and II).

To calculate the ion drag force we proceed as follows. As is usual in the BC approach, we accept the isotropic attractive Debye-Hückel (Yukawa) interaction potential between the ions and the grain. However, the effective screening length should be chosen appropriately. The value of the latter can be influenced by two factors: Plasma anisotropy related to the ion flow and strong ion-grain coupling related to the large grain sizes. Let us consider these factors separately.

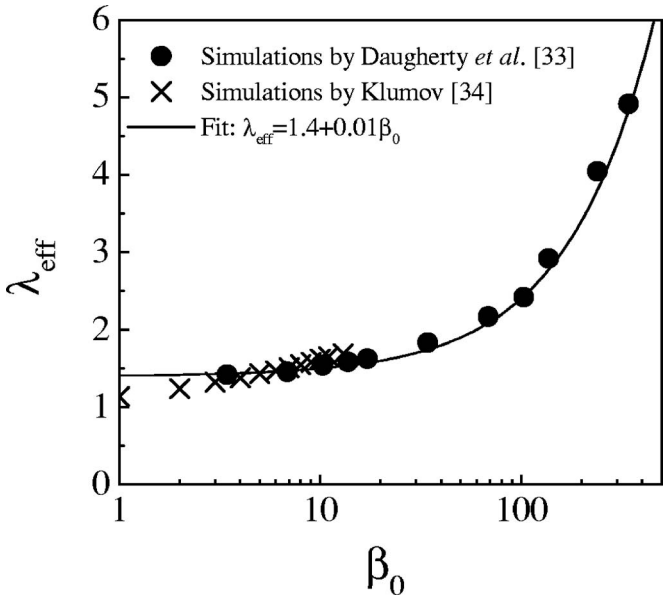

FIG. 4. Ratio of the effective plasma screening length to the ion Debye radius, $\lambda_{eff}=\lambda/\lambda_{Di}$, as a function of the scattering parameter $\beta_0=(e|\phi_s|/T_i)\times(a/\lambda_{Di})$. The symbols correspond to the best fit of the numerically obtained potential with the Debye-Hückel expression. The solid curve shows a linear fit used in this paper.

As has been demonstrated by Khrapak *et al.*,[32] the effective screening length (with respect to the calculation of the ion drag force acting on a small grain) is close to the linearized Debye radius for subthermal ion drifts and tends to electron Debye radius when the drift becomes highly suprathermal. Since in the considered case the ion drift is nearly thermal we neglect the effect of flow anisotropy on the screening length.

A much more important factor in our case is strong ion-grain coupling. Numerical simulations by Daugherty *et al.*[33] have demonstrated that the effective screening length is close to the linearized Debye radius for small grains ($a \ll \lambda_{Di}$), but increases with the grain size and reaches values on the order of the electron Debye radius for large grains ($a \gg \lambda_{Di}$). Since in our experiment the particle sizes are comparable to the linearized screening length (which is of the order of the ion Debye radius) this issue should be studied in more detail.

The increase of the effective screening length with grain size found in Ref. 33 is apparently a consequence of the increase in ion-grain coupling. This interpretation is supported by recent results of Ratynskaia *et al.*[34] who demonstrated that the value of the effective screening length is practically insensitive to separate values of grain size and surface potential, but depends only on their product through the scattering parameter. The results extracted from these two simulations[33,34] are summarized in Fig. 4, which shows the ratio of the effective screening length to the ion Debye radius $\lambda_{eff}=\lambda/\lambda_{Di}$ as a function of the "thermal" scattering

parameter $\beta_0=(e|\phi_s|/T_i)(a/\lambda_{Di})$. The numerical results are in reasonable agreement between each other, although they were obtained for quite different plasma conditions. A good fit in the range $2\lesssim\beta_0\lesssim500$ is provided by the expression $\lambda_{\text{eff}}=(1.4+0.01\beta_0)$. Below, we use this fit in evaluating the effective screening length λ.

To proceed further we estimate the value of the effective ("averaged" over velocities) scattering parameter β_{av}. Accounting for the ion flow we have

$$\beta_{\text{av}}=\frac{e|\phi_s|a}{\lambda T_i(1+u_0^2)}. \tag{2}$$

It turns out that the calculated values of β_{av} are in the range from ~16 to ~60; i.e., the ion-grain coupling is always strong even with the renormalized (increased) screening length. The momentum transfer in this regime has been investigated in detail in Refs. 19 and 22. The main feature of the ion scattering in this case comes from the existence of the barrier in the effective potential energy of ion-grain interaction. The barrier induces discontinuity in the dependence of the scattering angle on the impact parameter (see Fig. 2 of Ref. 19) at the transitional impact parameter ρ_*. Ion trajectories can be conveniently divided into two groups: (i) "Close collisions" ($\rho<\rho_*$)—the ions approach close to the grain (and if the distance of the closest approach is smaller than the grain radius they are collected) and are scattered with large angles growing monotonically from $\chi\to\pi$ at $\rho\to0$ to $\chi\to\infty$ at $\rho=\rho_*$; and (ii) "far collisions"—the ions do not approach close to the grain (the distance of the closest approach considerably exceeds λ) and the scattering angle decrease very fast from $\chi\to\infty$ at $\rho=\rho_*$ to $\chi\to0$. Careful analysis of the contribution from close and far collisions and proper account of the ion collection by the grain demonstrates that the momentum transfer cross section can be to a good accuracy estimated as[19,22]

$$\sigma(v)\approx\pi\rho_*^2, \tag{3}$$

where $\rho_*\approx\lambda[\ln\beta+1-(2\ln\beta)^{-1}]$. To calculate the ion drag force, the momentum transfer cross section should be integrated over the ion velocity distribution function: $\mathbf{F}_i=m_i\int\mathbf{v}vf_i(\mathbf{v})\sigma(v)d\mathbf{v}$. Using shifted Maxwellian distribution function for the ions, i.e., $f_i(\mathbf{v})=(2\pi v_{T_i}^2)^{-3/2}\exp[-(\mathbf{v}-\mathbf{u})^2/2v_{T_i}^2]$, and neglecting weak logarithmic velocity dependence of the cross section, we finally get the following expression for the ion drag force:

$$F_i\approx\sqrt{2\pi}n_im_iv_{T_i}^2(\rho_*)_{\text{av}}^2\left\{\sqrt{\frac{\pi}{2}}(2+u_0^2+u_0^{-2})\text{erf}\left(\frac{u_0}{\sqrt{2}}\right)+(u_0+u_0^{-1})\exp\left(-\frac{u_0^2}{2}\right)\right\}, \tag{4}$$

where $(\rho_*)_{\text{av}}\approx\lambda[\ln\beta_{\text{av}}+1-(2\ln\beta_{\text{av}})^{-1}]$. This expression is valid for collisionless plasmas with strong ion-grain coupling, where the ion drift velocity can be either subthermal or somewhat suprathermal.

V. DISCUSSION AND CONCLUSIONS

We compare the experimentally measured ion drag force F_i to theoretical calculations using formula (4). Our results are summarized in Fig. 3 and Tables I and II. Experimentally measured values of F_i are shown by solid circles and theoretical calculations are shown by open symbols. Our calculations reproduce the experimentally observed trend for the ion drag to increase with the discharge current and neutral gas pressure. The main contribution to this increase is due to the corresponding increase in the plasma density (see Tables I and II). The ion drag force also increases with grain size. The values of F_i are similar in experiment and theory, although formula (4) seems to underestimate the ion drag for the bigger particles [see Figs. 3(a) and 3(c)]. We attribute the better agreement between experiment and theory for smaller particles to the improved experimental accuracy due to smaller dispersion of their size. The scattering of theoretical values of F_i is due to experimental errors in measuring parameters that enter formula (4)—mainly the electric field E.

The theory outlined in this paper depends on a number of simplifying assumptions, e.g., isotropic interaction potential, effective screening length derived from simulations not accounting for the ion drift, shifted Maxwellian distribution of ions, and the use of the OML theory to calculate the particle surface potential. These assumptions are reasonable but all together could lead to increased uncertainty in the theoretical values of F_i. For this reason it would be important to compare our theory and experiment to a full-scale numerical simulation that is free of these assumptions. There is such a simulation for collisionless ions by Hutchinson using the specialized coordinate electrostatic particle and thermals in cell simulation code SCEPTIC.[35] Unfortunately, a detailed comparison is complicated by the fact that most of the reliable results from these simulations were obtained for drift velocities $u\gtrsim0.4c_{si}$ (due to difficulties to obtain converged SCEPTIC results at lower velocities), while the drift velocities considered in the present paper fall in the range of $0.1c_{si}\lesssim u\lesssim0.3c_{si}$ ($c_{si}=\sqrt{T_e/m_i}$ is the ion sound speed). Thus, experiments with higher drift velocities are required to make such a comparison valuable.

Finally, we verify that the electric force that acted on falling particles was much smaller than the ion drag force. The experimentally measured electric field and the ion drag force, as well as the particle surface potential calculated in Sec. IV are given in Tables I and II. The value of the particle charge number Z cannot be directly derived from the surface potential data since the grain size and plasma screening length are comparable and an ion flow is present; thus, a simple Coulomb expression does not hold. Still, a rough estimate $Ze\approx|\phi_s|a$ should be accurate within a factor of several. Using this estimate we found, for example, that for a discharge current of 1.4 A in argon at 0.6 mTorr, the electric force acting on the bigger particles was $F_E\approx4.4\times10^{-14}$ N, whereas the ion drag force was $F_i\approx5.4\times10^{-11}$ N. The ratio F_E/F_i estimated in this way was in the range of 0.21×10^{-3} to 4.1×10^{-3} in our experiment; therefore, the electric force can be neglected in the force balance.

To summarize, the ion drag force on micrometer-size

grains was experimentally measured in a low-pressure argon plasma in the regime of strong ion-grain coupling. Experimental results are compared to a theoretical model that extends the approach of Ref. 19 to the regime of suprathermal ions and gives a recipe for evaluating the effective screening length. A reasonable overall agreement is found between the experiment and theory.

ACKNOWLEDGMENTS

The work at the University of Iowa was supported by the U.S. Department of Energy Grant No. DE-FG02-04ER54795. S.A.K. was supported by DLR/BMBF Grant No. 50WP0203. The authors are grateful to B. Klumov for providing simulation results shown in Fig. 4.

[1] M. S. Barnes, J. H. Keller, J. C. Forster, J. A. O'Neill, and D. K. Coultas, Phys. Rev. Lett. **68**, 313 (1992).
[2] G. S. Selwyn and A. D. Bailey III, J. Vac. Sci. Technol. A **14**, 649 (1996).
[3] S. I. Krasheninnikov, Y. Tomita, R. D. Smirnov, and R. K. Janev, Phys. Plasmas **11**, 3141 (2004).
[4] D. Samsonov and J. Goree, Phys. Rev. E **59**, 1047 (1999).
[5] J. Goree, G. E. Morfill, V. N. Tsytovich, and S. V. Vladimirov, Phys. Rev. E **59**, 7055 (1999).
[6] K. Avinash, A. Bhattacharjee, and S. Hu, Phys. Rev. Lett. **90**, 075001 (2003).
[7] M. Klindworth, A. Piel, A. Melzer, U. Konopka, H. Rothermel, K. Tarantik, and G. E. Morfill, Phys. Rev. Lett. **93**, 195002 (2004).
[8] V. E. Fortov, A. G. Khrapak, S. A. Khrapak, V. I. Molotkov, and O. F. Petrov, Phys. Usp. **47**, 447 (2004).
[9] V. E. Fortov, A. V. Ivlev, S. A. Khrapak, A. G. Khrapak, and G. E. Morfill, Phys. Rep. **421**, 1 (2005).
[10] M. Kretschmer, S. A. Khrapak, S. K. Zhdanov, H. M. Thomas, G. E. Morfill, V. E. Fortov, A. M. Lipaev, V. I. Molotkov, A. I. Ivanov, and M. V. Turin, Phys. Rev. E **71**, 056401 (2005).
[11] D. R. Arifin, L. Y. Yeo, and J. R. Friend, Biomicrofluidics **1**, 014103 (2007).
[12] C. Zafiu, A. Melzer, and A. Piel, Phys. Plasmas **9**, 4794 (2002).
[13] C. Zafiu, A. Melzer, and A. Piel, Phys. Plasmas **10**, 1278 (2003); S. A. Khrapak, A. V. Ivlev, G. E. Morfill, H. M. Thomas, S. K. Zhdanov, U. Konopka, M. H. Thoma, and R. A. Quinn, Phys. Plasmas **10**, 4579 (2003); C. Zafiu, A. Melzer, and A. Piel, Phys. Plasmas **10**, 4582 (2003).
[14] M. Hirt, D. Block, and A. Piel, IEEE Trans. Plasma Sci. **32**, 582 (2004).
[15] M. Hirt, D. Block, and A. Piel, Phys. Plasmas **11**, 5690 (2004).
[16] K. Matyash, M. Fröhlich, H. Kersten, G. Thieme, R. Schneider, M. Hannemann, and R. Hippler, J. Phys. D **37**, 2703 (2004).
[17] V. Yaroshenko, S. Ratynskaia, S. Khrapak, M. H. Thoma, M. Kretschmer, H. Höfner, G. E. Morfill, A. Zobnin, A. Usachev, O. Petrov, and V. Fortov, Phys. Plasmas **12**, 093503 (2005).
[18] A. Piel (private communication).
[19] S. A. Khrapak, A. V. Ivlev, G. E. Morfill, and S. K. Zhdanov, Phys. Rev. Lett. **90**, 225002 (2003).
[20] R. A. Bosch and R. L. Merlino, Rev. Sci. Instrum. **57**, 2940 (1986).
[21] B. Liu, J. Goree, and V. Nosenko, Phys. Plasmas **10**, 9 (2003).
[22] S. A. Khrapak, A. V. Ivlev, G. E. Morfill, S. K. Zhdanov, and H. Thomas, IEEE Trans. Plasma Sci. **32**, 555 (2004).
[23] A. V. Ivlev, S. K. Zhdanov, S. A. Khrapak, and G. E. Morfill, Plasma Phys. Controlled Fusion **46**, B267 (2004).
[24] S. A. Khrapak, A. V. Ivlev, G. E. Morfill, and H. M. Thomas, Phys. Rev. E **66**, 046414 (2002).
[25] A. V. Ivlev, S. A. Khrapak, S. K. Zhdanov, G. E. Morfill, and G. Joyce, Phys. Rev. Lett. **92**, 205007 (2004).
[26] A. V. Ivlev, S. K. Zhdanov, S. A. Khrapak, and G. E. Morfill, Phys. Rev. E **71**, 016405 (2005).
[27] S. A. Khrapak, S. K. Zhdanov, A. V. Ivlev, and G. E. Morfill, J. Appl. Phys. **101**, 033307 (2007).
[28] L. S. Frost, Phys. Rev. **105**, 354 (1957).
[29] G. Lapenta, Phys. Rev. Lett. **75**, 4409 (1995).
[30] I. H. Hutchinson, Plasma Phys. Controlled Fusion **45**, 1477 (2003).
[31] E. C. Whipple, Rep. Prog. Phys. **44**, 1197 (1981).
[32] S. A. Khrapak, A. V. Ivlev, S. K. Zhdanov, and G. E. Morfill, Phys. Plasmas **12**, 042308 (2005).
[33] J. E. Daugherty, R. K. Porteous, M. D. Kilgore, and D. B. Graves, J. Appl. Phys. **72**, 3934 (1992).
[34] S. Ratynskaia, U. de Angelis, S. Khrapak, B. Klumov, and G. E. Morfill, Phys. Plasmas **13**, 104508 (2006).
[35] I. H. Hutchinson, Plasma Phys. Controlled Fusion **48**, 185 (2006).